Output Feedback H_∞ Preview Control of an Electro-Mechanical Valve Actuator

Lawrence Mianzo, *Member, IEEE,* and Huei Peng

***Abstract*— In an electro-mechanical valve actuated engine, solenoid actuators drive the valves that control airflow into the cylinders, allowing elimination of the camshaft and flexible control of the valve timing. Individual control of the valves provides flexibility in valve timing over all engine operating conditions and fully enables the benefits of variable valve timing. This paper describes a closed-loop preview control of an electro-mechanical valve actuator that achieves quiet, robust, and reliable operation in the presence of significant delays in electromagnetic system associated with eddy current losses. In this case, the desired trajectory of the armature position is known apriori. It is well know that preview control can greatly enhance disturbance rejection and tracking performance, when future information about the desired output is available. A detailed model is developed for the mechanical actuator system, the power electronics, and electro-magnetic system. Illustrative experimental results are also presented.**

***Index Terms*— Preview Control, Electro-Mechanical Valve Actuator, EMVA**

I. Introduction

MOST of today's automotive engines use valvetrain systems that couple the valve motion to crankshaft position through mechanical means via a belt or chain-driven, cam-based mechanisms. Although these systems provide reliable and accurate valve operation, the valve timings are inherently fixed and the resulting so-called fixed valve-timing engines cannot be operated in the most efficient manner over the entire range of engine operation. Recently, many studies [1]-[5] have shown that the flexibility in valve timing over all engine operating conditions provides significant benefits in fuel economy, emissions and torque performance. In an electro-mechanical valve actuated (EMVA) engine, a solenoid-based actuator drives the valves, providing variable valve timing capability and the camshaft is completely eliminated. This allows independent control of each valve, and freedom over valve opening and closing timing as well as duration. In terms of fuel economy, EMVA allows for reduced pumping loss (work required to draw air into the cylinder under throttled operation) via unthrottled operation by optimizing valve timing for load control. EMVA also facilitates valve and cylinder deactivation as well as creates the capability to fire less often than once per engine cycle. For emissions, EMVA allows flexible control of internal exhaust gas residual (by control of intake valve opening and exhaust valve closing) without the need for external gas re-circulation.

Manuscript received May 26, 2006.

L. Mianzo is with Visteon Corporation, H. Peng is with the University of Michigan.

Recently, there have been several papers on the modeling and control of variable valve timing electromagnetic actuators. In [6], a detailed model of the mechanical, electrical, and magnetic subsystem is described. A method for parameter identification and model correlation with experimental results was also shown. Another valuable reference with regard to modeling is [7]. Although this paper does not specifically refer to an electro-magnetic valve solenoid, many of the governing equations are the same, and there is a useful discussion about identifying the model nonlinearities. In [8], a tracking controller is described that uses a linear feedback term as well as an iterative learning control approach. In [9], a linear inner-loop output controller was used in conjunction with a cycle-to-cycle repetitive learning controller. In [10], a sensorless control approach is described that uses the current-voltage relationships and inflection points in the current to determine when the armature is close to the seating position. In [11] and [12] a linear plant model was developed that used system identification for determination of parameters. Linear optimal control was used to stabilize the actuator and improve performance. In [13] a nonlinear magnetic model was developed and validated experimentally. the dynamic mode of the system was used for development of a current pulse modulation control strategy. In [14] a method for reconstructing position from flux is proposed. An interesting sensitivity analysis is performed on the reconstructed position with respect to several types of uncertainty and modelling error. In [15], the work is extended to include optimization of the desired reference trajectory. In [16], a model-based control methodology is developed that uses position feedback along with a nonlinear observer that provides estimated armature velocity and current, and uses cycle-to-cycle learning. In [17] presents an observer based output feedback controller. The paper also breaks the model into a near model (valid close to the magnetic pole face) and a far model (valid elsewhere). In [18] Sontag's feedback is used to render the electromechanical valve actuator globally asymptotically stable. In [19] an extremum seeking controller uses a microphone measurement of sound intensity to tune a nonlinear feedback controller to reduce the magnitude of valve seating impacts. In [20], a subset of the electron-magnetic valve control problem is studied. The control focuses on the impacts that occur during the release phase of the valve opening due to valve lash configuration. Feedforward and iterative learning are used in the control approach.

All of the preceding literature focused on linear or direct acting electro-magnetic solenoids. This paper focuses on a lever-based actuator, where the valve is actuated through a lever-arm arrangement. The lever actuator has some inherent

advantages over a direct-acting actuator. The first is that due to construction of the pivot arm, which serves as a reinforcement to the armature structure, the armature can be laminated. These laminations serve to reduce eddy current losses in the system. In principle, the direct-acting actuator armature can be laminated, but in practice this is difficult without adding additional mass due to necessary reinforcements. The lever based design allows for the trade-off between transition energy and holding energy, and has a significant power consumption advantage over the direct-acting actuator. This is accomplished by adjusting the lever arm ratio in the design stage to allow for the reduced transition power consumption versus holding power consumption. This is important for opening against larger exhaust pressures in higher performance engines. A detailed model is developed for the mechanical lever actuator system and the power electronics, and electro-magnetic system.

With respect to the control approach, it has been shown that preview control can improve performance when future information about the desired output or exogenous disturbances is available. It is well known that non-minimum phase zeros and time delays impose a limit on achievable bandwidth of a control loop. This is due to the fact that non-minimum phase zeros can cause large peaks in the closed-loop sensitivity function if the controller bandwidth is increased. It can be seen from the Bode Sensitivity Integral that reducing the sensitivity at some frequencies will cause an increase in sensitivity at other frequencies [24]. On the other hand, as pointed out in [25], if a system has no time delays, no non-minimum phase zeros, small unstructured uncertainty, then there are no inherent limitations on bandwidth and tracking error can be made arbitrarily small.

Theoretically, perfect control can be achieved for a plant with a time delay or a non-minimum phase zero if a non-causal controller is used ([26], page 182). A non-causal controller is one in which future information is used. This is typically known as preview control. Preview control can be used to obtain performance beyond typical achievable performance obtained by a feedback only control design, much the way a pure feedforward controller allows an extra degree-of-freedom in the controller design. However, it was pointed out in [25] that the closed-loop sensitivity and the performance and stability robustness properties of the system are determined purely by the feedback portion of the control. This motivates the use of an H_∞ preview approach that takes advantage of the H_∞ framework for handling uncertainty and robustness issues while the preview control is used to improve the achievable controller bandwidth in systems with non-minimum phase zeros or time delays.

In this case, the desired trajectory of the armature position is known apriori. Therefore a closed-loop preview control approach of the electro-mechanical valve actuator is developed for quiet, robust, and reliable operation. The preview control is used to overcome significant system delays in the system.

II. System Modeling

In Fig. 1, a schematic of the actuator mechanical system is shown. In Fig. 2, a detailed free body diagram of the actuator

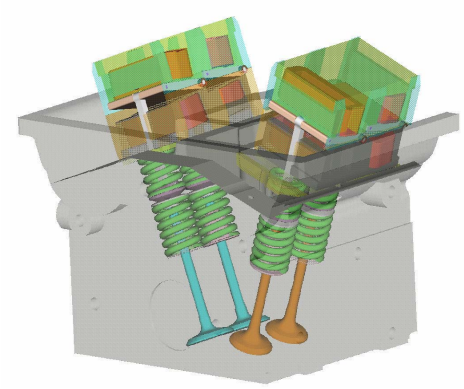

Fig. 1. Schematic of EMVA Actuator System

is presented. Two electro-magnets are used to capture and hold an armature. The armature rotates about a fixed pivot at point A. The armature is connected to a connecting rod at point C with a pin joint. The bottom portion of the armature connecting rod stem contacts the valve stem causing motion of the valve. There are two opposing springs which provide a restoring force, once the holding current is released. When there is no current in the electro-magnet coils, the equilibrium position of the armature is part-way between the electro-magnet coil pole faces. The equilibrium point of the valve is part-way between open and close. The exact equilibrium position depends on spacers and spring pre-loads. The valve opening and closing time, which is approximately 3 milliseconds, is determined mainly by the mechanical valve-armature-connecting-spring assembly mass and the spring stiffness and to some extent by the control action to softly seat the valve. In order to actuate the armature-valve assembly, the electromagnets are energized by passing current through the coils. This current generates electro-magnetic force in the magnetic circuit. The electromagnetic force attracts and is eventually used to capture the armature. It should be noted that changes in flux induced back-EMF voltage has an effect on the coil current rate of change. Once the armature is captured and is holding at the bottom pole face with the energized bottom (open) coil, the valve is fully open. To close the valve, the bottom coil is discharged and top (close) coil is energized. By proper timing of energizing/discharging of the coils, the valve is operated independent of the crankshaft position. By shaping the current waveform the armature/valve can also be seated softly which allows quiet operation and improved durability of the system.

Without any electro-magnetic force, the mechanical system nominally behaves as a second order mechanical system during most portions of the travel except when mechanical lash limits are reached. The valve and the armature connecting rod stem are two separate pieces that are kept together by the spring pre-load forces. The spacing, referred to as lash, is used between the valve and armature stems to guarantee that the valve will be completely seated even in the presence of worst-case thermal expansion. The two pieces separate close to the end of the closing event, once the valve is seated. Separation during

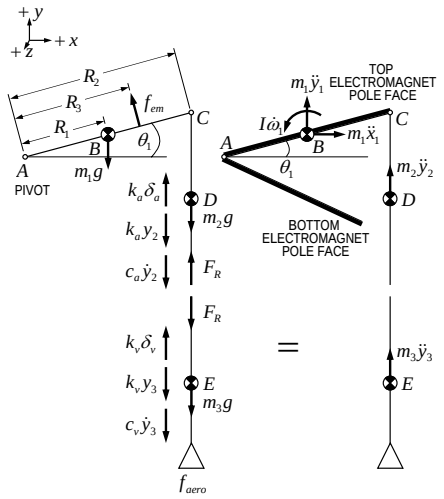

Fig. 2. Actuator Free Body Diagram

movement is also possible if the net force on a single piece exceeds the associated spring pre-load. Because during normal operation, the pre-load force is designed to prevent separation system, the system is modeled as a single mass term.

1) Mechanical System Equations of Motion: The equation of motion of the mechanical system is given by summing moments about point A:

$$\begin{aligned} &I_1\dot{\omega}_1 + R_1 cos\theta_1 m_1 \ddot{y}_1 - R_1 sin\theta_1 m_1 \ddot{x}_1 + R_2 cos\theta_1 m_2 \ddot{y}_2 \\ &= -k_a R_2 cos\theta_1 y_2 - c_a R_2 cos\theta_1 \dot{y}_2 \\ &-R_1 cos\theta_1 m_1 g - R_2 cos\theta_1 m_2 g \\ &+R_3 cos\theta_1 f_{em} + R_2 cos\theta_1 F_R + R_2 cos\theta_1 k_a \delta_a, \end{aligned} \tag{1}$$

where motion in the x direction of the connecting rod and valve stem is assumed negligible. Here θ_1, ω_1, $\dot{\omega}_1$ are the angular position, velocity, and acceleration of the armature. And R_1 is the length of the armature between the pivot A and the armature center of gravity at B. Here R_2 is the length of the armature between the pivot A and the connecting rod pin C. And where I_1 is the moment of inertia of the armature about the axis of rotation, z, m_1 is the mass of the armature, and m_2 is the effective mass of the connecting rod. Also, k_a is the armature connecting rod spring stiffness, c_a is the damping coefficient, f_{em} is the electromagnetic force, and g is the acceleration due to gravity. δ_a is the initial displacements of the armature. F_R is the reaction force between the connecting rod and the valve stem. From the velocity and acceleration analysis, the relevant coordinate transformations between the angular and linear positions are given by

$$\ddot{x}_1 = -\dot{\omega}_1 R_1 sin\theta_1 - \omega_1^2 R_1 cos\theta_1, \tag{2}$$

where $\ddot{x}_1$ is the linear acceleration in the x direction at the armature center of gravity at point B. Additionally,

$$\ddot{y}_1 = \dot{\omega}_1 R_1 cos\theta_1 - \omega_1^2 R_1 sin\theta_1, \tag{3}$$

where $\ddot{y}_1$ is the linear acceleration in the y direction at the armature center of gravity at point B. Also,

$$y_2 = R_2 sin\theta_1, \tag{4}$$

where y_2 is the linear displacement of the connecting rod center of gravity in the y direction at point D, and by the time derivatives of y_2 given as $\dot{y}_2 = \omega_1 R_2 cos\theta_1$ and $\ddot{y}_2 = \dot{\omega}_1 R_2 cos\theta_1 - \omega_1^2 R_2 sin\theta_1$. Substituting (2) through (4) into (1) and simplifying to obtain

$$\begin{aligned} &I_1\dot{\omega}_1 + m_1 R_1^2 \dot{\omega}_1 + m_2 R_2^2 cos^2\theta_1 \dot{\omega}_1 \\ &-m_2 R_2^2 \omega_1^2 sin\theta_1 cos\theta_1 = -k_a R_2^2 sin\theta_1 cos\theta_1 \\ &-c_a R_2^2 cos^2\theta_1 \omega - R_1 cos\theta_1 m_1 g + R_2 cos\theta_1 F_R \\ &-R_2 cos\theta_1 m_2 g + R_2 cos\theta_1 k_a \delta_a + R_3 cos\theta_1 f_{em}. \end{aligned} \tag{5}$$

The equation of motion for the valve is obtained by summing the forces in the vertical direction

$$m_3 \ddot{y}_3 = -c_v \dot{y}_3 - k_v y_3 - m_3 g + k_v \delta_v - F_R + f_{aero}, \tag{6}$$

where m_3 is the effective mass of the valve, k_v is the valve spring stiffness, c_v is the damping coefficient, δ_v is the initial deflection of the valve spring, and f_{aero} is the aerodynamic force acting on the valve. Also, y_3, $\dot{y}_3$, and $\ddot{y}_3$ are the linear displacement, velocity, and acceleration in the y direction of the valve at the center of gravity. When the valve and armature connecting rod are moving together $y_3 = R_1 sin\theta_1$, $\dot{y}_3 = \omega_1 R_1 cos\theta_1$, and $\ddot{y}_3 = \dot{\omega}_1 R_2 cos\theta_1 - \omega_1^2 R_2 sin\theta_1$. Substituting into (6) to obtain

$$\begin{aligned} &m_3(\dot{\omega}_1 R_2 cos\theta_1 - \omega_1^2 R_2 sin\theta_1) \\ &= -c_v \omega_1 R_1 cos\theta_1 - k_v R_1 sin\theta_1 + f_{aero} \\ &-m_3 g + k_v \delta_v - F_R. \end{aligned} \tag{7}$$

Solving (7) for F_R and substituting into (5) and noting that from equilibrium for the combined system, $-R_1 cos\theta_1 m_1 g - R_2 cos\theta_1 (m_2 + m_3) g + R_2 cos\theta_1 (k_a \delta_a + k_v \delta_v) = 0$, to obtain the equation of motion for the combined system

$$\begin{aligned} &I_1\dot{\omega}_1 + m_1 R_1^2 \dot{\omega}_1 + (m_2 + m_3) R_2^2 cos^2\theta_1 \dot{\omega}_1 \\ &-(m_2 + m_3) R_2^2 \omega_1^2 sin\theta_1 cos\theta_1 \\ &= -(k_a + k_v) R_2^2 sin\theta_1 cos\theta_1 - (c_a + c_v) R_2^2 cos^2\theta_1 \omega_1 \\ &+R_3 cos\theta_1 f_{em} + R_2 cos\theta_1 f_{aero}. \end{aligned} \tag{8}$$

Here the combined effective mass of the mechanical system includes the mass of the valve, armature and connecting rod, one third of the spring masses [22], and the spring locks and retainers (not shown).

2) Linearized Mechanical Modeling: The system in Equation (8) can be written as a function of the state vector, x, and the input, u. Here the state vector is $x = [\theta, \omega]$ and input vector is $u = [f_{em}, f_{aero}]$. The function $f(x, u)$ can be expressed

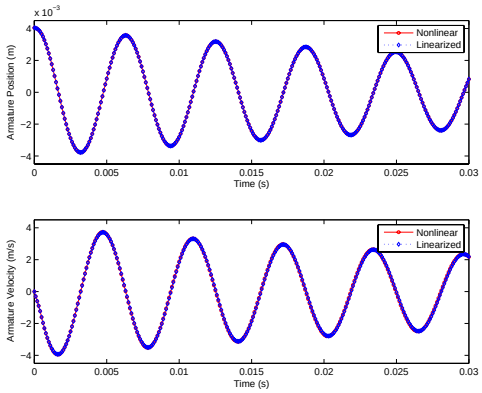

Fig. 3. Nonlinear and Linearized Model Comparison, Free Response

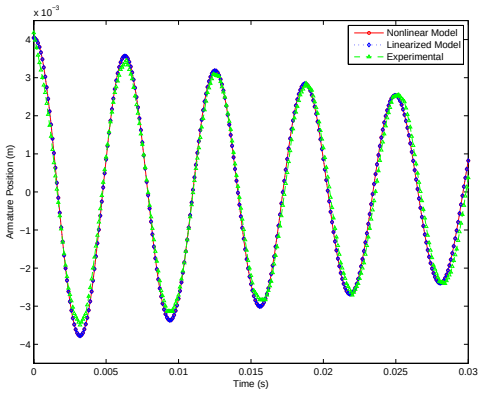

Fig. 4. Model and Experimental Comparison, Free Response

as

$$f(x,u)$$
$$= f(\bar{x},\bar{u}) + \tfrac{df(x,u)}{dx}|_{\bar{x},\bar{u}} \cdot \tilde{x} + \tfrac{df(x,u)}{du}|_{\bar{x},\bar{u}} \cdot \tilde{u} + H.O.T. \quad (9)$$
$$\cong \tfrac{df(x,u)}{dx}|_{\bar{x},\bar{u}} \cdot \tilde{x} + \tfrac{df(x,u)}{du}|_{\bar{x},\bar{u}} \cdot \tilde{u},$$

where $\bar{x}$ and $\bar{u}$ are the constant equilibrium values of the state and input vectors, and $\tilde{x}$ and $\tilde{u}$ are their perturbed values. It should be noted that $f(\bar{x},\bar{u}) = 0$ at equilibrium. Performing the linearization on (8) to obtain model linearized about the equilibrium point

$$[I_1 + m_1R_1^2 + (m_2+m_3)R_2^2]\tilde{\ddot{\theta}}_1 + (c_a+c_v)R_2^2\tilde{\dot{\theta}}_1 + (k_a+k_v)R_2^2\tilde{\theta}_1 = R_3\tilde{f}_{em} + R_2\tilde{f}_{aero}. \quad (10)$$

Equation (10) can be written as

$$\tilde{\ddot{\theta}}_1 + 2\zeta\omega\tilde{\dot{\theta}}_1 + \omega^2\tilde{\theta}_1 = \tfrac{R_3}{I_{eff}}\tilde{f}_{em} + \tfrac{R_2}{I_{eff}}\tilde{f}_{aero}, \quad (11)$$

where ω is the natural frequency, given by

$$\omega = \sqrt{\tfrac{(k_a+k_v)R_2^2}{I_1+m_1R_1^2+(m_2+m_3)R_2^2}}, \quad (12)$$

and ζ is the damping factor, given by

$$\zeta = \tfrac{1}{2\omega} \cdot \tfrac{(c_a+c_v)R_2^2}{I_1+m_1R_1^2+(m_2+m_3)R_2^2}, \quad (13)$$

and I_{eff} is given by

$$I_{eff} = I_1 + m_1R_1^2 + (m_2+m_3)R_2^2. \quad (14)$$

3) Correlation Results: A model of the EMVA system was developed using Matlab/Simulink. The model has been parameterized using CAE analysis and experimental data for obtaining damping coefficients. In Fig. 3, a comparison between the nonlinear mechanical model and the model that has been linearized about the equilibrium point has been shown. It can be seen that linearized model matches very closely with the nonlinear model. The full nonlinear model will continue to be used for design verification, but it is clear that the linearized model can be used for continued control and diagnostics development. In Fig. 4, a comparison of the free response for the Simulink model and experimental data is shown. The moment of inertia, spring, and geometric parameters were obtained analytically, but the damping coefficients were obtained from experimental data. The correlation between model and experimental data is quite good, but there appears to be some slight mismatch in the natural frequency possibly due to variations in mass or spring characteristics or due to approximations of spring mass into lumped parameter mass.

4) Power Electronics and Electro-Magnetic Modeling: A schematic of the power electronics is shown in Fig. 5. The power electronics are a switched circuit and there are four modes of operation, depending on the state of the high-side and low-side switches, Q_1 and Q_2, respectively. If the low-side switch is on and the high-side switch is off, the current will increase slowly. Because the slow current increase draws only from the low voltage supply, the high voltage rail is unaffected. The flux rate of change, $\frac{d\lambda}{dt}$, is given by

$$\tfrac{d\lambda}{dt} = V_{LV} - iR, \quad (15)$$

where V_{LV} is the input voltage provided by the vehicle power supply, i is the current in the electromagnet coil, and R is the coil resistance. The magnetic flux, λ, is a nonlinear function of current and armature angular position, θ_1. For the purposes of control-oriented modeling, this relationship is typically treated as a static map. An alternative would be to perform a co-simulation between the lumped parameter model in Matlab, and more detailed magnetic analysis packages, but for the purpose of this study and for control development, the static mapping was used. The relationship is given by

$$\lambda = \lambda(i,\theta_1). \quad (16)$$

Equation (16) can be inverted to obtain a relationship for current in terms of λ and θ_1

$$i = I(\lambda,\theta_1). \quad (17)$$

Substituting (17) into (15) to obtain

$$\tfrac{d\lambda}{dt} = V_{LV} - I(\lambda,\theta_1)R. \quad (18)$$

If the low-side switch is on and the high-side switch is on, the current will increase rapidly. Since the rapid current increase uses the high voltage rail capacitor, the high voltage rail will also be depleted. The flux rate of change is given by

$$\tfrac{d\lambda}{dt} = V_{LV} - I(\lambda,\theta_1)R + \tfrac{1}{C_1}\int i_{c1}dt, \quad (19)$$

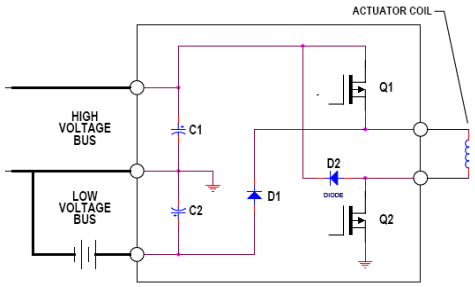

Fig. 5. Integrated Amplifier and High Voltage Power Supply

where C_1 is the high voltage capacitor. If the low-side switch is off and the high-side switch is on, then the current will simply free-wheel through the circuit and the current in the coil will decrease slowly due to losses in the circuit. In this case the flux rate of change is given by

$$\frac{d\lambda}{dt} = -I(\lambda, \theta_1)R. \tag{20}$$

If the low-side switch is off and the high-side switch is off, the current will decrease rapidly, A rapid current decrease puts energy back into the high voltage reservoir, thereby increasing or boosting the high voltage reservoir. The expression for flux rate of change is this case is given by

$$\frac{d\lambda}{dt} = V_{LV} - I(\lambda, \theta_1)R - \frac{1}{C_1}\int i_{c1}dt. \tag{21}$$

Noting that $V_{HV} = \frac{1}{C_1}\int i_{c1}dt$, Equations (18)-(21) can be represented as a single equation, depending on the state of the high-side and low-side switches, Q_1 and Q_2, respectively, and is given by

$$\frac{d\lambda}{dt} = V_{in} - I(\lambda, \theta_1)R. \tag{22}$$

where V_{in} and the relationship with Q_1 and Q_2 is given by

$$\begin{array}{llll} Q_1 = 0, & Q_2 = 1, & V_{in} = & V_{LV} \\ Q_1 = 1, & Q_2 = 1, & V_{in} = & V_{LV} + V_{HV} \\ Q_1 = 0, & Q_2 = 0, & V_{in} = & V_{LV} - V_{HV} \\ Q_1 = 1, & Q_2 = 0, & V_{in} = & 0 \end{array} \tag{23}$$

The electromagnetic force, f_{em}, is a function of the current and the armature angular position and is given by

$$f_{em} = f_{em}(i, \theta_1). \tag{24}$$

Substituting (17) into (24) to obtain an equation only in λ, and θ_1

$$f_{em} = f_{em}(\lambda, \theta_1). \tag{25}$$

III. Control Approach

To write the Equations (11) and (22) as a system of first-order ordinary differential equations, the following state variables are defined: x_1 is the armature angular position of the linearized model, x_2 is the armature angular velocity, and x_3 is the electro-magnet flux. The control input, u, is the input voltage, V_{in}. Equations (11) and (22) can then be written as a system of first order ordinary differential equations as follows

$$\dot{x}_1 = x_2 \tag{26}$$

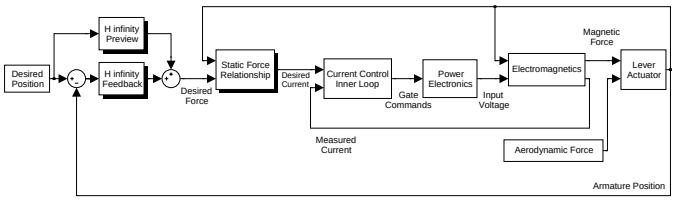

Fig. 6. Actuator Control Partitioning

$$\dot{x}_2 = -2\zeta\omega x_2 - \omega^2 x_1 + \frac{R_3}{I_{eff}}\tilde{f}_{em}(x_1, x_3) + \frac{R_2}{I_{eff}}\tilde{f}_{aero} \tag{27}$$

$$\dot{x}_3 = u - I(x_3, x_1)R. \tag{28}$$

$$y = x_1 \tag{29}$$

The overall control system is divided into an inner and an outer loop as shown in Figure 6. The outer loop determines a desired magnetic force for a desired armature profile. It is assumed that the inner loop switching feedback control is sufficiently fast and delivers the desired magnetic force. The outer loop calculates the desired force that is required to be delivered by the inner loop and deals with the simplified system

$$\dot{x}_1 = x_2 \tag{30}$$

$$\dot{x}_2 = -2\zeta\omega x_2 - \omega^2 x_1 + \frac{R_3}{I_{eff}}\tilde{f}_{em} + \frac{R_2}{I_{eff}}\tilde{f}_{aero} \tag{31}$$

For the system of Equations (30) and (31), a H_∞ preview control law is used to determine the desired magnetic force. Preview is used because the desired position trajectory is calculated apriori and to overcome force generation delays due to eddy current losses and inductive dynamics. It is difficult to model the eddy current losses analytically, so it will be approximated as a n sample pure delay. The inner loop uses a switching control law to determine the power amplifier gate switch commands (amplifier input voltage at each time step) to deliver the desired force. The switching control law is as follows

$$\begin{array}{lll} \sigma < 0 & & V_{LV} - V_{HV} \quad Volts \\ \sigma = 0 & u = & 0 \quad Volts \\ \sigma > 0 & & V_{LV} + V_{HV} \quad Volts \end{array} \tag{32}$$

where

$$\sigma = i_d - i_a, \tag{33}$$

and where i_d is the desired electromagnet coil current and i_a is the achieved coil current, which is obtained from measurement. No deadband is currently used, but one could be added to tune the voltage switching and resulting current ripple. i_d is determined by the H_∞ preview outer loop [23]. The preview control law is a Hamiltonian based formulation which allows an additional design degree of freedom and the simultaneous design of feedback and preview control components. A static mapping is then used to determine the desired magnetic force based on the desired coil current and the desired armature angular position.

To design the preview control law for the outer loop, the augmented plant LFT is formed, using the structure of Figure 7. The control law block is not shown to emphasis that the LFT is written for the system from the output of the control

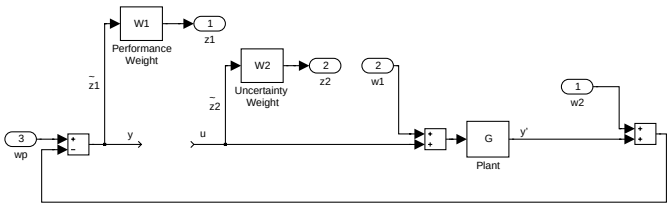

Fig. 7. EMVA Actuator Augmented Plant without Feedback Term

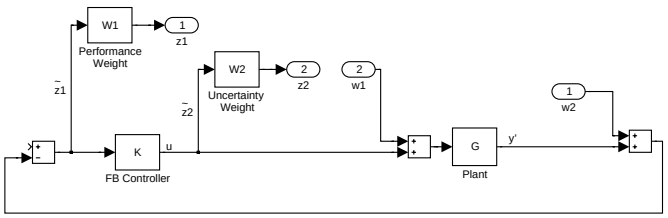

Fig. 8. EMVA Actuator Augmented Plant with Feedback Term

to the input of the control. The LFT is formed by writing the state equations, outputs, z_1 and z_2, and measurement (input to the controller), y, in terms of the states, x, the disturbances, w_1 and w_2, control, u, and preview signal, w_p. The input to the control, y, should not be confused with the output of the plant, y'. The continuous time plant of Equations (30) and (31) can be discretized and written in state-space form as

$$\tilde{x}(k+1) = \tilde{a}\tilde{x}(k) + \tilde{b}u_f(k) \tag{34}$$

with the position measurement, y'

$$y'(k) = \tilde{c}\tilde{x}(k) \tag{35}$$

There is a delay in the force generation due to eddy current losses in the magnetic coil. The eddy current delay tends to behave like a pure delay. There is another component of delay due to the inductance of the coil, as modeled by Equation (22). This behaves more like nonlinear dynamic inductive delay, rather than a pure delay. The standard feedback term can typically compensate for the inductive delay, but cannot so readily compensate for the eddy current loss delay. The preview control law is effective in dealing with this delay. This is because the preview control uses future information about the desired trajectory of the valve to overcome limitations on achievable bandwidth of a control loop. The typical delay due to eddy current losses was 300-400 microseconds. The outer control loop was running at 100 microseconds. A delay of 5 time steps was used to include the eddy current delay as well as the control update delays. Assuming an integer delay of d time steps, the delayed force can be written as

$$u_f(k+d) = u_c(k) \tag{36}$$

where $u_c(k)$ is the input command force, and $u_f(k)$ is the generated force. The delayed plant can be written as

$$x(k+1) = ax(k) + bu_c(k) \tag{37}$$

with measurement

$$y'(k) = cx(k) \tag{38}$$

The state-space representation of the performance weight, W_1, as shown in Figure 7, can be written as

$$\begin{aligned} x_1(k+1) &= a_1x_1(k) + b_1(w_p(k) - y'(k) - w_2(k)) \\ &= a_1x_1(k) + b_1w_p(k) - b_1w_2(k) - b_1cx(k) \end{aligned} \tag{39}$$

with the output z_1

$$z_1(k) = c_1x_1(k) \tag{40}$$

The uncertainty weight can be expressed as

$$x_2(k+1) = a_2x_2(k) + b_2u(k) \tag{41}$$

with the output z_2

$$z_2(k) = c_2x_2(k) + d_2u(k) \tag{42}$$

The augmented plant can be written as a LFT as

$$\begin{aligned} &\left[\begin{array}{c} x(k+1) \\ x_1(k+1) \\ x_2(k+1) \\ \hline z_1(k) \\ z_2(k) \\ \hline y(k) \end{array}\right] \\ &= \left[\begin{array}{ccc|ccc|c} a & 0 & 0 & 0 & 0 & b & 0 \\ -b_1c & a_1 & 0 & 0 & -b_1 & 0 & b_1 \\ 0 & 0 & a_2 & 0 & 0 & b_2 & 0 \\ \hline 0 & c_1 & 0 & 0 & 0 & 0 & 0 \\ 0 & 0 & c_2 & 0 & 0 & d_2 & 0 \\ \hline -c & 0 & 0 & 0 & -I & 0 & I \end{array}\right] \left[\begin{array}{c} x(k) \\ x_1(k) \\ x_2(k) \\ \hline w_1(k) \\ w_2(k) \\ \hline u(k) \\ \hline w_p(k) \end{array}\right] \\ &= \left[\begin{array}{c|c|c|c} A & B_1 & B_2 & B_p \\ \hline C_1 & D_{11} & D_{12} & D_{1p} \\ \hline C_2 & D_{21} & D_{22} & D_{2p} \end{array}\right] \left[\begin{array}{c} x(k) \\ x_1(k) \\ x_2(k) \\ \hline w_1(k) \\ w_2(k) \\ \hline u(k) \\ \hline w_p(k) \end{array}\right] \end{aligned} \tag{43}$$

Consider only the feedback term as shown in Figure 8. To form the transfer function between w and z, we first obtain the relationship for y'

$$y' = G(u + w_1) = GK(-y' - w_2) + Gw_1 \tag{44}$$

Rearranging to get

$$y' = -SGKw_2 + SGw_1 \tag{45}$$

where the sensitivity, S, is defined as $S := (I+GK)^{-1}$. Now writing the relationship for $\tilde{z}_1$

$$\tilde{z}_1 = -y' - w_2 \tag{46}$$

Substituting Equation (45) into (46)

$$\tilde{z}_1 = SGKw_2 - SGw_1 - w_2 \tag{47}$$

Noting that

$$SGKw_2 - w_2 = (SGK - S(I + GK))w_2 = -Sw_2 \tag{48}$$

Then Equation (48) can be simplified to

$$\tilde{z}_1 = -SGw_1 - Sw_2 \tag{49}$$

Writing z_1 after the weighting function

$$z_1 = -W_1 SGw_1 - W_1 Sw_2 \tag{50}$$

Next writing the expression for $\tilde{z}_2$, where $\tilde{z}_2 = u$

$$\tilde{z}_2 = K(-y' - w_2) = -KSGw_1 - KSw_2 \tag{51}$$

Writing z_2 after the weight function

$$z_2 = -W_2 KSGw_1 - W_2 KSw_2 \tag{52}$$

Finally, writing the transfer function from w to z in matrix form

$$\begin{aligned}\begin{bmatrix} z_1 \\ z_2 \end{bmatrix} &= \begin{bmatrix} -W_1 SG & -W_1 S \\ -W_2 KSG & -W_2 KSw_2 \end{bmatrix} \begin{bmatrix} w_1 \\ w_2 \end{bmatrix} \\ &= \begin{bmatrix} T_{zw} \end{bmatrix} \begin{bmatrix} w_1 \\ w_2 \end{bmatrix}\end{aligned} \tag{53}$$

As can be seen from Equation (53), for the feedback term, the sensitivity function can be shaped with the W_1 weighting. The uncertainty can be modeled with the W_2 weighting.

From [23], for the system in Equation(43), the preview approach minimizes the transfer function between the disturbance, $w(k)$, and the performance criteria, $z(t)$. Additionally, the preview term of the resulting controller requires future information of previewable disturbance, in other words, $w_p(k)$ is known over the interval $[k, k + N_{la}]$, where N_{la} is the number of preview steps.

If the cost function to be minimized is $J = \frac{1}{2}\sum_0^{N_f}[z'z - \gamma^2 w'w]$. The Hamiltonian is then

$$\begin{aligned}H(x, \lambda, k) = \tfrac{1}{2}[z(k)'z(k) - \gamma^2 w(k)'w(k)] + \\ \lambda(k+1)'(Ax(k) + B_1 w(k) + B_2 u(k) + B_p w_p(k))\end{aligned} \tag{54}$$

Differentiating Equation (54) with respect to u and w, the optimal condition can be achieved if we have

$$\tfrac{dH}{dw(k)} = -\gamma^2 Iw(k) + B_1'\lambda(k+1) = 0 \tag{55}$$

and

$$\tfrac{dH}{du(k)} = u(k) + B_2'\lambda(k+1) + D_{12}'D_{1p}w_p(k) = 0 \tag{56}$$

The costate equation is

$$\lambda(k) = \frac{\partial H}{\partial x(k)} = C_1'C_1 x(k) + A'\lambda(k+1) + C_1'D_{1p}w_p(k) \tag{57}$$

with the final condition, $\lambda(N_f) = 0$, where N_f is the final sample of interest. Solving Equation (55) and (56) for u and w and substituting into the state and costate equation, the resulting equations can then be written in matrix form as

$$\begin{aligned}\begin{bmatrix} x(k+1) \\ \lambda(k) \end{bmatrix} \\ = \begin{bmatrix} H_\infty \end{bmatrix} \begin{bmatrix} x(k) \\ \lambda(k+1) \end{bmatrix} + \begin{bmatrix} H_{p\infty} \end{bmatrix} \begin{bmatrix} w_p(k) \end{bmatrix}\end{aligned} \tag{58}$$

where

$$\begin{bmatrix} H_\infty \end{bmatrix} := \begin{bmatrix} A & \gamma^{-2}B_1B_1' - B_2B_2' \\ C_1'C_1 & A' \end{bmatrix} \tag{59}$$

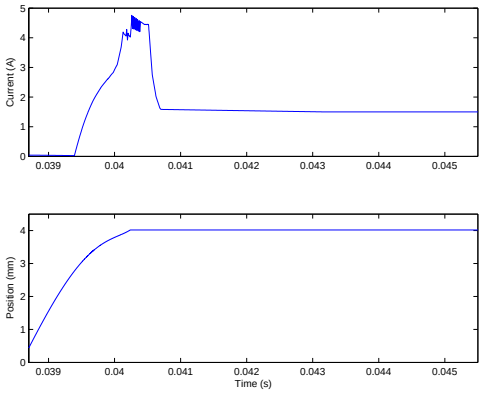

Fig. 9. EMVA Actuator Control Simulation Results

which is the standard H_∞ discrete Hamiltonian matrix, and

$$\begin{bmatrix} H_{p\infty} \end{bmatrix} := \begin{bmatrix} B_p - B_2 D_{12}' D_{1p} \\ C_1' D_{1p} \end{bmatrix} \tag{60}$$

which is the the preview component of the Hamiltonian matrix.

Equation (58) forms a discrete two point boundary value problem, with mixed boundary conditions. A solution for the costate dynamics is assumed:

$$\begin{aligned}\lambda(k) = X_\infty(k)x(k) + \sum_{n=0}^{N_{la}-1} F_1(k,n)w_p(k+n) \\ + F_2(k)w_p(k+N_{la})\end{aligned} \tag{61}$$

From the assumed solution, the outer loop H_∞ preview control law can be obtained (see [23] for additional details)

$$\begin{aligned}\begin{bmatrix} \hat{x}(k+1) \\ u(k) \end{bmatrix} \\ = \begin{bmatrix} A + B_1F_\infty + Z_\infty L_\infty C_2 + B_2F_\infty & -Z_\infty L_\infty \\ F_\infty & 0 \end{bmatrix} \begin{bmatrix} \hat{x}(k) \\ y(k) \end{bmatrix} \\ + \begin{bmatrix} B_2 f_1(w_p(k)) + B_p w_p(k) + B_1 f_2(w_p(k)) \\ - Z_\infty L_\infty (D_{2p}w_p(k) + D_{21}f_2(w_p(k))) \\ f_1(w_p(k)) \end{bmatrix}\end{aligned} \tag{62}$$

where A, B_1, B_2, B_p, C_1, etc. are defined in Equation (43). The first term on the right hand side of Equation (62) is the standard discrete-time H_∞ output feedback term. F_∞ and L_∞ are the discrete-time H_∞ control and estimator gains, respectively, defined as $F_\infty := -B_2'[I - X_\infty\gamma^{-2}B_1B_1' - B_2B_2')]^{-1} \cdot X_\infty A$ and $L_\infty := -A'Y_\infty[I - (\gamma^{-2}C_1C_1' - C_2C_2')Y_\infty]^{-1}C_2'$. Z_∞ is defined as $Z_\infty := (I - \gamma^{-2}Y_\infty X_\infty)^{-1}$, where X_∞ is the solution of the discrete-time full information Riccati equation and Y_∞ is the solution of the discrete-time full control Riccati equation. The second term on the right hand side of Equation (62) is the preview term, where

$$\begin{aligned}f_1(w_p(k)) = -B_2'[I - X_\infty(\gamma^{-2}B_1B_1' - B_2B_2')]^{-1} \\ \cdot[X_\infty(B_p - B_2D_{12}'D_{1p})w_p(k) \\ + \sum_{n=0}^{N_{la}-1} F_1(k+1,n)w_p(k+1+n) \\ + F_2(k+1)w_p(k+1+N_{la})] - D_{12}'D_{1p}w_p(k)\end{aligned} \tag{63}$$

and

$$f_2(w_p(k)) = \gamma^{-2}B_1'[I - X_\infty(\gamma^{-2}B_1B_1' - B_2B_2')]^{-1} \cdot[X_\infty(B_p - B_2D_{12}'D_{1p})w_p(k) + \sum_{n=0}^{N_{la}-1} F_1(k+1,n)w_p(k+1+n) + F_2(k+1)w_p(k+1+N_{la})] \quad (64)$$

The output feedback term and X_∞ and Y_∞ can be obtained from one of the Matlab discrete-time H_∞ solvers of the μ-Analysis and Synthesis Toolbox or the Robust Control Toolbox. X_∞ and Y_∞ can then be used in the construction of the preview control term. As pointed out by one of the anonymous reviewers, in recent years, it has been determined that a better numerical approach is to solve the H_∞ problem using LMIs. With respect to the theoretical development, the preview law developed was based on a solution of the dual Riccati approach. A direction for possible future work is to extend the theoretical development of the preview control law into a LMI based development.

The control algorithm is demonstrated in simulation on the full nonlinear model in Figure 9. Typical parameters used were total moving mass (m_2+m_3) of 0.0868 Kg, I_{eff} of 1.0305e-004 $[Kg-m^2]$, total spring rate (k_a+k_v) of 134 KN/m, damping rate ζ of 0.0172, transition time of 3.2 milliseconds, R_1 of 0.0117 m and R_2 of 0.0280 m. The coil resistance was 1-2 Ohms, and the magnetic characteristics were obtained from detailed magnetic modeling programs and experimental data for verification. Because of the nonlinearities in the magnetics, unstructured uncertainty was used to model the performance and uncertainty weights. Also, to keep the controller order small for high speed implementation on the DSP, low order weightings were chosen. For the uncertainty weight, 20 percent modeling uncertainty was allowed at low frequency while 100 percent modeling uncertainty was allowed at frequencies above the mechanical bandwidth of the the system, with a smooth transition in between. The performance weighting was chosen to provide approximately 10 percent error within the mechanical bandwidth, but performance was allowed to degrade at higher frequencies.

The control algorithm was implemented in a Texas Instruments TMS320LF2812 running at an outer loop sample rate of 100 microseconds. The algorithm uses feedback of position and current to directly control the gates of the power electronics. The feedback and preview control is operational during the valve transition. Once the valve is seated, the control switches to a constant current to provide some additional holding force margin to prevent the valve from unseating due to engine vibration of aerodynamic forces. The feedback control by itself could not provide reliable operation of the lever actuator. When running the feedback only control, the valve could not be reliably seated in a repeatable fashion, and the feedback-only controller would often lose control of the armature and the valve would not properly seat. The valve could only be operated in a robust fashion with some type of feedforward control, due to the large delays in the force generation. The preview control provides good actuator response in overcoming the significant delays due to eddy current losses in the electromagnetic system.

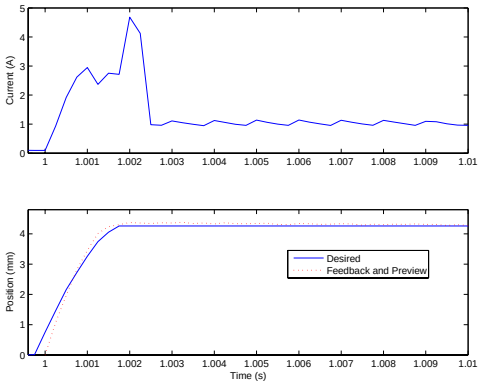

Fig. 10. EMVA Actuator Control Experimental Results

The experimental results for the controller are shown in Figure 10. It can be noted from the current trace that there is a current peak due prior to the valve seating. This is due to the fact that the spring restoring force provides most of the restoring force during the transition. As the armature comes close to reaching the opposite electro-magnet, the armature and valve assembly begin to slow, a large force is required to ensure that the armature does not begin to move away, causing the valve to seat. Once the valve is seated, the control switches to a constant current. With the preview control, there is some impact and noise when the valve seats. However, this noise level was under the noise level due to engine operation and induction noise and was deemed acceptable in a jury evaluation during normal engine operation. Due to the significant delays of 300-400 microseconds resulting from eddy current losses and due to the large inductance of the electromagnetic coil, the feedback only control is not successful in controlling the actuator. The preview control behaves like a look-ahead feedforward control. And feedforward is necessary to overcome the limitations of electromagnetic system. Alternatively, a delay could be included in the controller order, but doing so decreases the controller robustness. Preview does not degrade the closed loop control robustness, but does rely on having a model of reasonable fidelity.

IV. Conclusion

In this paper, a preview control approach is developed for the successful control of an EMVA actuator. A detailed model of the mechanical linkage, electro-magnetic properties, and control and power electronics is developed. The full simulation model is correlated against experimental data, and a linearized model of the system shows good agreement with the full model. A H_∞ preview control approach is developed, and experimental results show good performance of the actuator control.

References

[1] Assanis D.N. and Bolton B.K., "Variable Valve Timing Strategies for Optimum Engine Performance and Fuel Economy," *Proceedings of the Energy Sources Technology Conference and Exhibition*, 1994.

[2] Lenz H.P., Wichart K., and Gruden D., "Variable Valve Timing - A Possibility to Control Engine Load without Throttle," *SAE Paper 880288*, 1988.
[3] Schecter M.M. and Levin M.B., "Camless Engine," SAE Paper 960581, 1996.
[4] Tuttle J.H., "Controlling Engine Load by Means of Late Intake Valve Closing," *SAE Paper 800794*, 1980.
[5] Tuttle J.H., "Controlling Engine Load by Means of Early Intake Valve Closing," *SAE Paper 820408*, 1982.
[6] Wang, Y., Stefanopoulou, A., Haghgooie, M., Kolmanovsky, I., and Hammoud, M., "Modeling of an Electromechanical Valve Actuator for a Camless Engine," *5th International Symposium on Advanced Vehicle Control*, Ann Arbor, Michigan, USA, 2000
[7] Vaughan, N. D. and Gamble, J. B., "The Modelling and Simulation of a Proportional Solenoid Valve," American Society of Mechanical Engineers, *1990 Proceedings of the Winter Annual Meeting*, Dallas, Texas, USA, Nov 25-30 1990
[8] Hoffmann, W. and Stefanopoulou, A. G., "Iterative Learning Control of Electromechanical Camless Valve Actuator," *Proceedings of the American Control Conference*, June 2001
[9] Tai, C., Stubbs, A., and Tsao, T. C.,"Modeling and Controller Design of an Electromagnetic Engine Valve," *Proceedings of the American Control Conference*, June 2001
[10] Butzmann, S., Melbert, J., and Koch, A., "Iterative Learning Control of Electromechanical Camless Valve Actuator," *Proceedings of the American Control Conference*, June 2001
[11] Tai, C., Tsao, T., "Control of an Electromechanical Camless Valve Actuator," Proceedings of the American Control Conference, v 1, 2002, p 262-267
[12] Tai, C., Tsao, T., "Quiet seating control design of an electromagnetic engine valve actuator American Society of Mechanical Engineers," Dynamic Systems and Control Division (Publication) DSC, v 70, 2002, p 157-164
[13] Xiang, Y., "Modeling and Control of a Linear Electro-Mechanical Actuator (LEMA) for Operating Engine Valves," Conference Record - IAS Annual Meeting (IEEE Industry Applications Society), v 3, 2002, p 1943-1949
[14] Ronchi, F., Rossi, C., Tilli, A., "Sensing Device for Camless Engine Electromagnetic Actuators," IECON Proceedings (Industrial Electronics Conference), v 2, 2002, p 1669-1674
[15] Montanari, M., Ronchi, F., Rossi, C., Tonielli, A., "Control of a Camless Engine Electromechanical Actuator: Position Reconstruction and Dynamic Performance Analysis," IEEE Transactions on Industrial Electronics, v 51, n 2, April, 2004, p 299-311
[16] Wang, Y., Megli, T., Haghgooie, M., Peterson, K., and Stefanopoulou, A., "Modeling and control of Electromechanical Valve Actuator," SAE 2002-01-1106
[17] Peterson, K., Stefanopoulou, A., Megli, T., Haghgooie, M., "Output Observer Based Feedback for Soft Landing of Electromechanical Camless Valvetrain Actuator," Proceedings of the American Control Conference, v 2, 2002, p 1413-1418
[18] Peterson, K. S., Stefanopoulou, A. G., "Rendering the Electromechanical Valve Actuator Globally Asymptotically Stable Peterson," Proceedings of the IEEE Conference on Decision and Control, v 2, 2003, p 1753-1758
[19] Peterson, K. S., Stefanopoulou, A. G., "Extremum Seeking Control for Soft Landing of an Electromechanical Valve Actuator," Automatica, v 40, n 6, June, 2004, p 1063-1069
[20] Peterson, K., Stefanopoulou, A., Wang, Y., Megli, T., "Virtual Lash Adjuster for an Electromechanical Valve Actuator through Iterative Learning Control," American Society of Mechanical Engineers, Dynamic Systems and Control Division (Publication) DSC, v 72, n 1, 2003, p 295-301
[21] Haskara, I., Kokotovic V., and Mianzo, L. A., "Control of an Electro-Mechanical Valve Actuator for a Camless Engine," *International Journal of Robust Control*, 2002
[22] Sears, F., Zemansky, M., Young, H., "University Physics, 5th Edition", Section 11.5, Addison Wessley Publishing Company
[23] Mianzo, L. A., "A Unified Hamiltonian Framework For H2 And H-Infinity Preview Control Algorithms With Application To A Variable Valve Timing Engine," University of Michigan Ph.D. Dissertation, 2002
[24] Freudenber, J. S. and Looze, D.,"Right Half Planes Poles and Zeros and Design Tradeoffs in Feedback Systems," *IEEE Transactions on Automatic Control*, 1985
[25] Middleton, R. H., Freudenberg, J. S., and McClamrock, N. H., "Sensitivity and Robustness Properties in the Preview Control of Linear Non-Minimum Phase Plants," *Proceedings of the American Control Conference*, June 2001
[26] Skogestad, S. and Postlethwaite, I., Multivariable Feedback Control, Wiley, 1996

Lawrence Mianzo Lawrence Mianzo received his B.S. from the University of Pittsburgh, M.S. from Penn State University, and Ph.D. from the University of Michigan, all in Mechanical Engineering. He is currently a Research Scientist in Advanced Powertrain Electronic Systems at Visteon Corporation. His research interest are in powertrain and vehicle control systems, driver assistance and awareness systems, and collision warning systems. He has 10 patents issued and was named one of the 2002 MIT Technology Review Magazine 100 Top Young Innovators.

Huei Peng Huei Peng received his Ph.D. in Mechanical Engineering from the University of California, Berkeley in 1992. He is currently a Professor in the Department of Mechanical Engineering, and the Director of Automotive Engineering Program of the University of Michigan, Ann Arbor. His research interests include adaptive control and optimal control, with emphasis on their applications to vehicular and transportation systems. He has been an active member of SAE and the ASME Dynamic System and Control Division. He has served as the chair of the ASME DSCD Transportation Panel from 1995 to 1997. He is currently an Associate Editor for the ASME Journal of Dynamic Systems, Measurement and Control. He received the National Science Foundation (NSF) Career award in 1998.